HAL
archives-ouvertes.fr

Formation of TiO2 nanostructures modified Eumelanin films with enhanced properties for biopolymer implementations

Mushtaq Ali, Muhammad Saad, Mamatimin Abbas, Arshad Bhatti, Luca Ottaviano, Marianna Ambrico, Andrea Di Cicco, Roberto Gunnella

▶ **To cite this version:**

HAL Id: hal-03014061
https://hal.archives-ouvertes.fr/hal-03014061

Submitted on 19 Nov 2020

1   # Formation of TiO$_2$ nanostructures modified Eumelanin films with

2   # enhanced properties for biopolymer implementations

3   _____

4   Mushtaq Ali [a,b,*], Muhammad Saad [c], Mamatimin Abbas [d], Arshad S. Bhatti [e], Luca Ottaviano [a],

5   Marianna Ambrico [f], Andrea Di Cicco [g], and Roberto Gunnella [g,h]

6   [a] Dipartimento di Scienze Fisiche e Chimiche (DSFC), Università dell'Aquila, Via Vetoio 10 67100

7   L'Aquila, Italy

8   [b] Department of Physics, HITEC University, Taxila Cantt, Pakistan

9   [c] Institute of Physics, Kazan Federal University, Kazan, 420008 Russia

10   [d] CNRS, Université Bordeaux, Bordeaux INP, Laboratoire de l'Intégration du Matériau au Système (IMS), UMR 5218, 16

11   Avenue Pey-Berland, 33607 Pessac Cedex, France

12   [e] Department of Physics, COMSATS University Islamabad, 45550, Pakistan

13   [f] CNR-Istituto di Nanotecnologia Via Amendola 122/D, I-70126 Bari, Italy

14   [g] School of Science and Technology, University of Camerino, Via Madonna delle Carceri 62032 Camerino (MC),

15   Italy

16   [h] INFN sez, Perugia Via A. Pascoli 06123 Perugia, Italy

17

18

19

20   [*] Corresponding author.

21   E. mail address: mushtaqali.zada@gmail.com (M.Ali)

22

23

24

25

26

27

28

Abstract

Thin films of hybrid melanin-TiO_2 nanoparticles (eumelanin: TiO_2) deposited from solution by electro-spray were accurately inspected to unveil modified structural and electronic properties for device implementations. Based on the reorganization of the melanin electronic valence orbital, among other interesting behaviors, we observed up to a two orders increase in the absorption coefficient in the visible range. Furthermore the red-shifted absorption features, disclose that the extended π- stacking of oligomers is mainly responsible for the tunability of the optical gap as confirmed by photoluminescence. TiO_2 nanostructures via oxidative polymerization, further improve the oligomeric character observed by means of Raman scattering. Finally, the photocatalytic activity of TiO_2 nanoparticles helps the saturation of shallow trap states in melanin structure and consequently enhances the charge carrier transport.

40

41

42

44

45

46

47

48

49

50

51

52

53

54

1. Introduction

The recent advancements in the research of pigments like eumelanin (termed as melanin) are preluding to applications of these biopolymers in the fields of bioelectronics, sensors, and (opto)electronic devices [1-4]. Among the main physicochemical properties of melanin are the well-known strong UV-Vis optical absorption, relatively high ionic/electronic conductivity, photoconductivity (PC), exceptional biocompatibility, antioxidant and free-radical scavenging activities [3,5,6]. They are at the basis of the diverse functions of the natural melanin in the human body as a photoprotective agent and its involvement in some diseases like melanoma skin cancer, Parkinson's and Alzheimer neurodegenerative disease. However for study purpose and applications point of view, synthetic melanin guarantees a more convenient and reliable model instead of natural melanin due to inherent heterogeneity and difficulty in separation of the latter one [3,5]. Monomeric units of melanin structure are sketched in Fig. 1: (a) 5-6-dihydroxyindole (DHI or HQ), (b) 5,6-dihydroxyindole-2-carboxylic acid (DHICA), (c) indolequinone (IQ), and (d) semichinone (SQ), further details about melanin structure can be found elsewhere [3,6,7]. Previous studies started from characteristics of pellet type melanin samples [3], and subsequently developed in various directions, allowed the study of the secondary structure and the dependence of functional properties on the molecular organization and film quality [4,7,8]. Comprehensive results were obtained in terms of film smoothness, continuity and overall quality, followed by controlled structural, electronic and optoelectronic properties that have connected the fundamental features of the melanin organization, its feasible functionalizations [5,6,9] and practical applications [3,10-13].

An intriguing aspect of this research is involving the interactions of melanin with other organic or inorganic nanoparticles in hybrid/nanocomposite materials. Most common drawbacks are complete insolubility in organic solvents, the lack of appropriate deposition techniques that prevent the development of homogeneous and reproducible blended thin films, and the lack of a solid conceptual frame to understand the structure–property–function relationships upon the interaction of nanoparticles with synthetic melanin, hindering the full implementation of the bio(electronic) devices.

Titanium dioxide (TiO_2) nanoparticles are low cost, non-toxic, stable oxide semiconductor with distinctive physical and chemical properties, applied in some photovoltaic devices and several

85 photocatalysts applications. The combination of metal/metal oxide nanoparticles like TiO_2 with
86 organic structured materials is very attractive for the electronic, morphological properties
87 modifications [14-17] and towards practical applications. To date, the formation of hybrid
88 functional materials based on TiO_2 and monomer precursors, like DHICA were established using
89 different synthesis methods i.e., DHICA polymerization through coated TiO_2 nanoparticles and
90 solution mixed DHICA/TiO_2 hybrid nanostructures [18,19], but complete picture of such hybrid
91 materials in the form of thin films, ideal to investigate nanohybrid materials is still lacking.
92 Hence, melanin-TiO_2 nanostructure is an open issue for understanding the mechanism of hybrid
93 formation, as their properties are strongly dependent on the particle size and aggregation
94 mechanisms that vary while passing from solution to the solid film.

95 Here, we report the fabrication of melanin blended TiO_2 nanoparticle thin films by solution
96 processed electrospray deposition (ESD) technique. The aim to develop thin films of these kind
97 of hybrid nanostructures was multifold: the foremost, is to enhance the photo absorption for
98 extended range of wavelength by exploiting the broadband absorption of melanin and TiO_2
99 nanoparticles. Also important is the response of melanin coupled to strong electron
100 acceptor/donor materials. Last but not least, the structure-function relation and mutual
101 dependence of these components must be critically investigated. By the way, properties of
102 melanin (particularly the transport) are complicated by the presence of two kinds of water, the
103 weakly and strongly bounded to the structure [3,6,9]. Adding the TiO_2 which has been widely
104 used for water splitting, purification or treatment applications will bring experimental
105 insights for the charge transport mechanisms and its response towards charge carrier
106 recombination activities. In addition, the motivation of this work was to explore in details the
107 characteristics of melanin and melanin: TiO_2 nanoparticle active layers, when heated at a high
108 temperature as required for many device preparations (T> 120°C). To investigate all these issues,
109 we analyzed morphological, structural, electrical and optical properties of the active layer
110 melanin and blend (melanin: TiO_2) thin films for as prepared and treated samples, grown by ESD
111 deposition technique looking forward to organic/inorganic photovoltaics and other
112 (bio)electronic device applications.
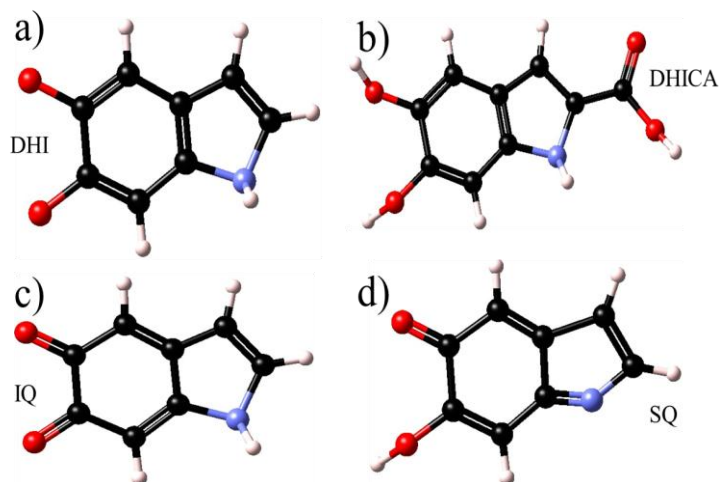
Fig. 1. Monomeric units for melanin structure: (a) DHI or HQ, (b) DHICA, (c) IQ, (d) SQ. Red (oxygen atoms), light blue (nitrogen atoms), white (hydrogen atoms), and black (carbon atoms).

2. Experimental details

Synthetic melanin powder, prepared by oxidation of tyrosine with hydrogen peroxide (M8631 synthetic melanin) and TiO_2 nanoparticles (about 25 nm) were purchased from Sigma-Aldrich. Melanin is notoriously insoluble pigment, but dimethyl sulfoxide (DMSO) is the most effective solvent for its use. We dissolved melanin in Dimethyl Sulfoxide Methanol Solution (DMSO: CH_3OH; 1:20) with the concentration of 0.2 mg/ml. Similarly, for TiO_2 solution we used the same concentration of 0.2 mg/ml but different solvent (dichlorobenzene). After the preparation of the solution, the melanin and melanin: TiO_2 (with 1:1 ratio) were deposited by electrospray technique[4] on indium-tin-oxide (ITO) and corning glass substrates. To realize the formation of hybrid nanostructures through enhanced interfaces area the melanin and TiO2 proportion were kept the same, without going into the details of ratio optimization, which is essential for the purpose of efficient electronic devices in the future and is beyond the scope of this paper.

The schematic of ESD developed system [20,21] during thin films deposition is presented in the Fig. 2. A solution container was pressurized with the N_2 gas and the flow rate was controlled by measuring the time required to move a solution of 20 μL through 1 cm gap marked at various position on Teflon tube. The flow rate (1.3 $\mu L/s$) and applied voltage (2 kV) were kept constant during the deposition [6]. ESD melanin and blend films of the average thickness of 200 nm on

glass and ITO substrates were characterized with various microscopic and spectroscopic techniques.
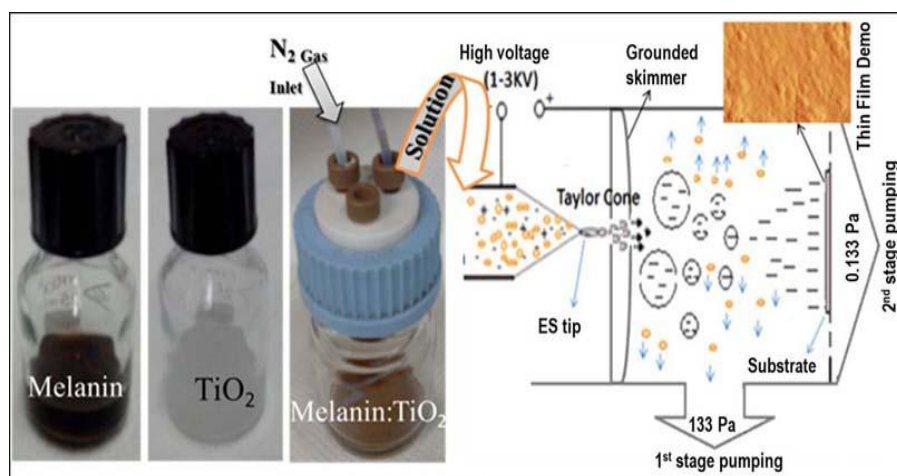
Fig. 2. Schematic of the ESD system used for the film growth on respective substrates.

The morphological studies of these melanin and blend films were performed by Scanning Electron Microscopy (SEM- SU-1500 Hitachi) operating at 2–5 kV and Atomic Force Microscopy (AFM- Agilent's Pico Plus) working in tapping mode with cantilever frequency 160 kHz. The AFM images were analyzed quantitatively by Gwyddion Software [22]. Optical absorption spectra of melanin and blend films were measured in the ultraviolet, visible and near infrared regions. Absorption measurements were carried out by measuring the absorption light intensity obtained by spectrophotometer (Perkin, Elmer Lambda 950 UV/Vis/NIR). Photoluminescence (PL) study was carried out by using Dongwoo Optron W500i with He-Cd laser having wavelength 325 nm (3.8 eV) for excitation purpose.

The identification and investigation of functional group vibrations of melanin and blend (melanin: TiO_2) were performed using NICOLET 6700 Fourier Transform infrared spectroscopy (FTIR). Argon ion laser with laser lines, of wavelength 514 nm as excitation source was used in dark ambient at room temperature for Raman spectra (Renishaw 1000). Finally, the electrical characterization was taken under the dark and illumination conditions. The current–voltage (J – V) curves were obtained by using a Keithley 4200 semiconductor analyzer in dark and under illumination of an AM1.5 (100 mW/cm^2) calibrated with IL1400BL radiometer. Gold stripes were evaporated with a channel length of 50μm onto glass substrates after film deposition to get

155 planar geometry for J – V measurements in both forward and backward voltage sweep directions.

156

3. Results and discussion

3.1. Film morphology

159 The morphology of synthetic melanin film is quite different and of better quality than that of
160 natural melanin, due to the successive improvements in the methods of fabrication and the choice
161 of solvents that affect the structure, and thin film quality [8,23,24]. In the present work, we
162 report the thermal heat treatment effect on the morphology of synthetic melanin film and of its
163 blend with TiO_2 nanoparticles. Previously [6], we found that the pure melanin thin films
164 deposited at 3 kV applied voltage by ESD technique showed 2D regions with separated
165 boundaries between flat zones formed on sample surface due to strain and to the process of
166 drying. Therefore, here in this work we effectively lowered the applied voltage to 2 kV, for all
167 the samples. SEM analysis show that the thin films fabricated at 2 kV by controlled electrospray
168 deposition process [6,20] are quite homogenous, with complete flat coverage of the substrate
169 with planar regular structures without any cracks or boundaries as shown in Fig. 3(a-d). SEM
170 images for the annealed (at 120° C for 5 minutes) samples deposited on glass were presented in
171 Fig. 3(a and b) for melanin and melanin: TiO_2 blended films respectively, while same annealed
172 samples deposited on ITO substrate are in Fig. 3(c and d). Annealing is particularly important in
173 the case of the hybrid films, to reach an acceptable homogeneity. The pristine hybrid film on ITO
174 substrate (not shown here) indicated small clusters of TiO_2 nanoparticles coated and /or wrapped
175 by melanin polymorphic organized layers. After annealing, the homogeneity of the blend film
176 enhanced significantly and moderate distribution of TiO_2 nanoparticles (Fig. 3(b and d)) on the
177 whole substrate was observed. Thermal annealing certainly affects the uniformity of thin films
178 deposited on all kinds of substrates especially the conducting surfaces. In discussing samples
179 deposited on glass substrates (upper panel) vs. samples on ITO substrates (lower panel) in Fig.3,
180 the latter ones probably exhibited more wetting character in the blend film, preferentially due to
181 the interaction between melanin and titania nanoparticles or interfaces with the substrate. These
182 observations are favorable to conditions of molecular orbital hybridization and functionalization
183 to be employed in real devices.

184
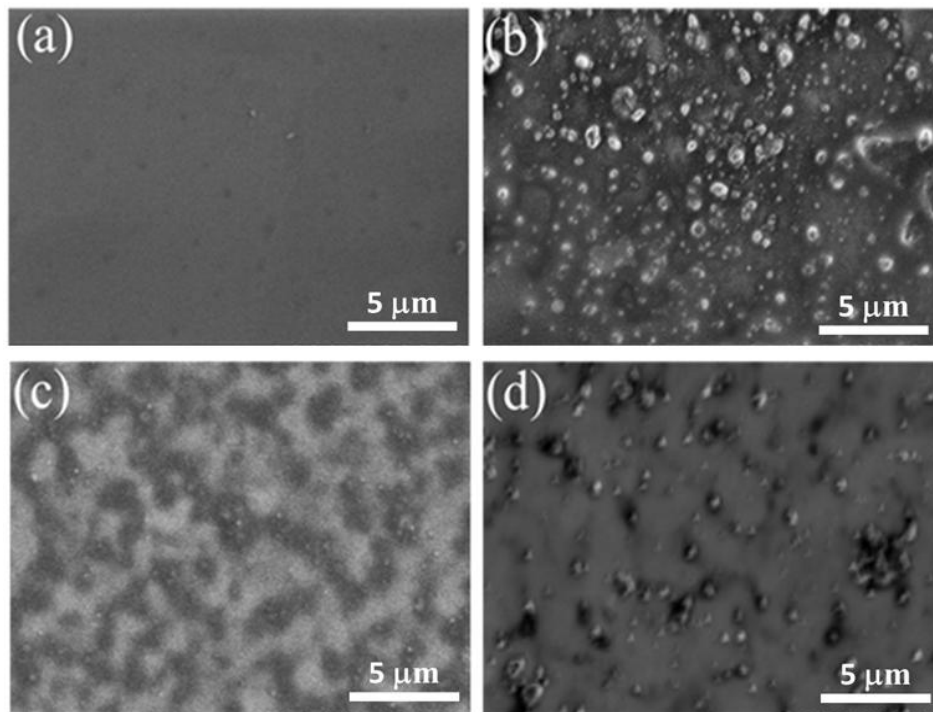
Fig. 3. SEM images comparison: (a) melanin film on glass substrate; (b) blend (melanin: TiO$_2$) on glass substrate; (c) melanin film on ITO substrate; (d) blend (melanin: TiO$_2$) on ITO substrate. Furthermore, all SEM images were from samples annealed at 120° C.

AFM images of melanin and blend (melanin: TiO$_2$) deposited on glass (upper panel) and ITO substrate (lower panel), after heat treatment are reported in Fig. 4, respectively. While comparing annealed melanin thin films grown on ITO with those on glass substrates, the first one shows clear improvement in the surface morphology, in terms of film roughness, homogeneity and oligomers structures planarity, as shown in Fig. 4(a and c). AFM images of blended titania films annealed at 120°C are reported in Fig. 4(b and d). Thermal annealing might affect polymers film thickness, by a more organized molecular spacing and in addition, helping supramolecular aggregation with increased uniformity and film quality. It is evidenced from the images that the signatures of titania nanoparticles are very clear, especially on ITO substrates, and showed almost no difference in root-mean-square roughness (before annealing 1.02 nm – after annealing 1.05 nm) associated with different regions of the blend film after annealing. In case of melanin films in the left panels of Fig. 4, the morphology disclosed overall uniform lengthened platelet [6,8]. Compared to the latter, slightly corrugated surface of melanin: TiO$_2$ samples (right panel of Fig. 4) was observed when blended with polymers by solution process, obviously due to
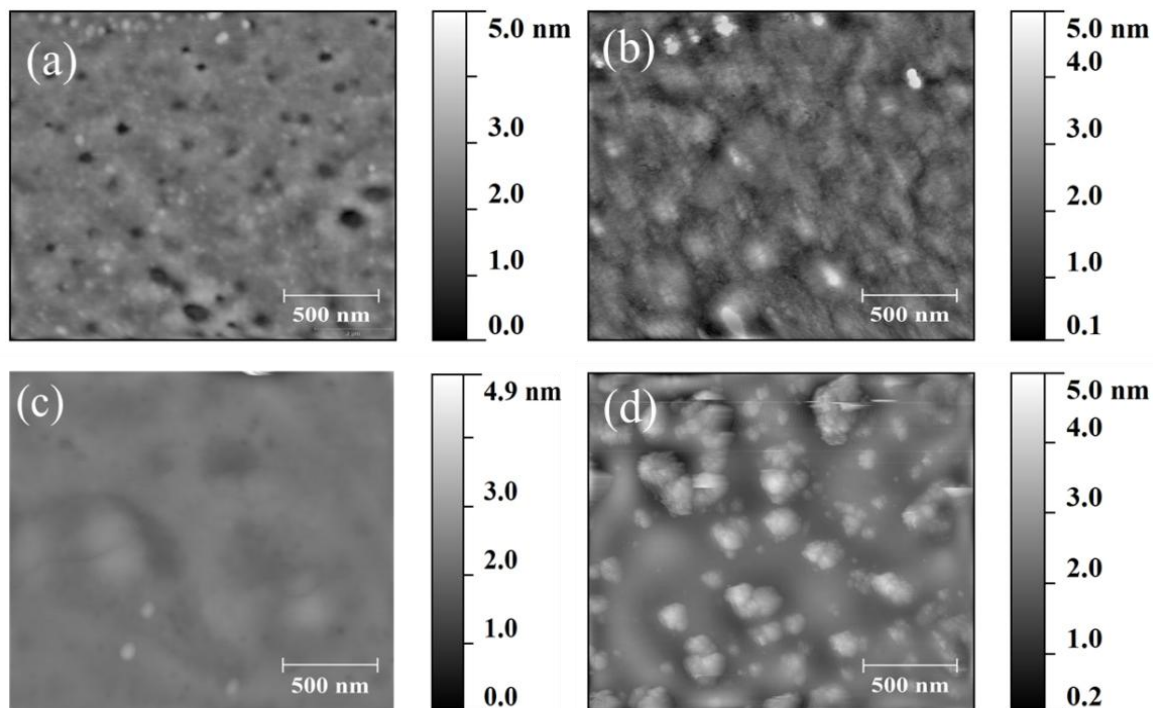
Fig. 4. AFM images in tapping mode of melanin thin film deposited on glass substrate (a), and melanin: TiO$_2$ blend on glass substrate (b) - (upper panel). AFM image of melanin thin film deposited on ITO substrate (c), and blend (melanin: TiO$_2$) deposited on ITO substrate (d) - (lower panel). Here, we presented the samples annealed at 120° C.

3.2. Optical absorption

The normalized absorption spectra of thin films melanin and its blend with TiO$_2$ as prepared on glass and ITO substrates were determined in the region (300- 950 nm) and shown in the Fig. 5(a and b), respectively. Before annealing the absorption spectra of melanin, particularly on glass substrates (Fig. 5(a), solid curve), showed the typical wide band character consisting of overall featureless smooth absorption without any apparent edge. However, an increase in absorption spectra in the visible wavelength range (380-750 nm) observed for pure melanin films, after annealing (Fig. 5(a and b), solid and dot curves) is suggesting more compacts films (especially on conducting substrate, probably due to adhesion properties of melanin [25,26]), and improved

self–assembly relating to monomeric components bonding. The most intriguing results were obtained after embedding TiO_2 nanoparticles in the melanin matrix particularly on conducting surfaces. The blended (melanin: TiO2) dash and dash dot curves in Fig. 5(a and b) show enhanced absorption spectra compared to melanin, due to the photocatalytic activity of TiO2 nanoparticles and better mutual adhesion during the ESD process [21,27]. Moreover, the normalized absorption spectra of melanin blending TiO_2 nanoparticles on ITO substrates showed (Fig. 5b) completely twisted behavior composed of new features different from the melanin characteristic broadband monotonic absorption [3,5]. These spectra with even broader and dominant absorption (350-800 nm) are similar to the prominent absorption of conventional low band gap conducting polymers in the range of 400-750 nm due to π-π^* bonding [15,20]. The peak observed near UV region at about 350 – 400 nm is due to the fundamental absorption of the Ti-O bond at that wavelength as shown in the inset of Fig. 5(a). Moreover, the wet nature of ESD thin films on ITO substrates reflect the slow growth rate for the dynamics of molecular organization/oligomerization, as compared to the fast growth rate on non-wet insulating glass substrates. These effects on conducting substrates were also accompanied by slight differences in morphology observed in SEM and AFM analysis. In addition, the photocatalytic properties of TiO_2 nanoparticles also played a significant role in the DHICA/DHI polymerization [19] that alters the absorption spectra of melanin in a different fashion from that of amorphous semiconductor [3]. Although melanin layer absorption features on conducting surface in the UV-Vis-NIR range are in agreement with the previous experimental observations [4] and theoretical simulations [28,29], and attributed to an increase in the degree of π- stacking and to the oxidation state of melanin, we emphasize here that the presently observed physical properties are the consequence of a controlled film fabrication by efficient ESD system able to blend melanin with TiO_2 nanoparticles which leads to a photocatalytic oxidative action on conducting surface. These examined absorption features are enhanced under thermal annealing with an increase of two orders of magnitude of absorption coefficient around 600 nm (Fig. 5b) in comparison to pure melanin suggesting the augmented adhesion between the two constituents. In fact, melanin similar to polydopamine [17,25] shows significantly strong adhesion to TiO_2 nanoparticles in the hybrid structure due to catechol groups.

We recently applied the Tauc model [4,24,30,31] for the calculation of energy gap value from the optical band edge as the absorption curve is not showing any of the exponential behavior of
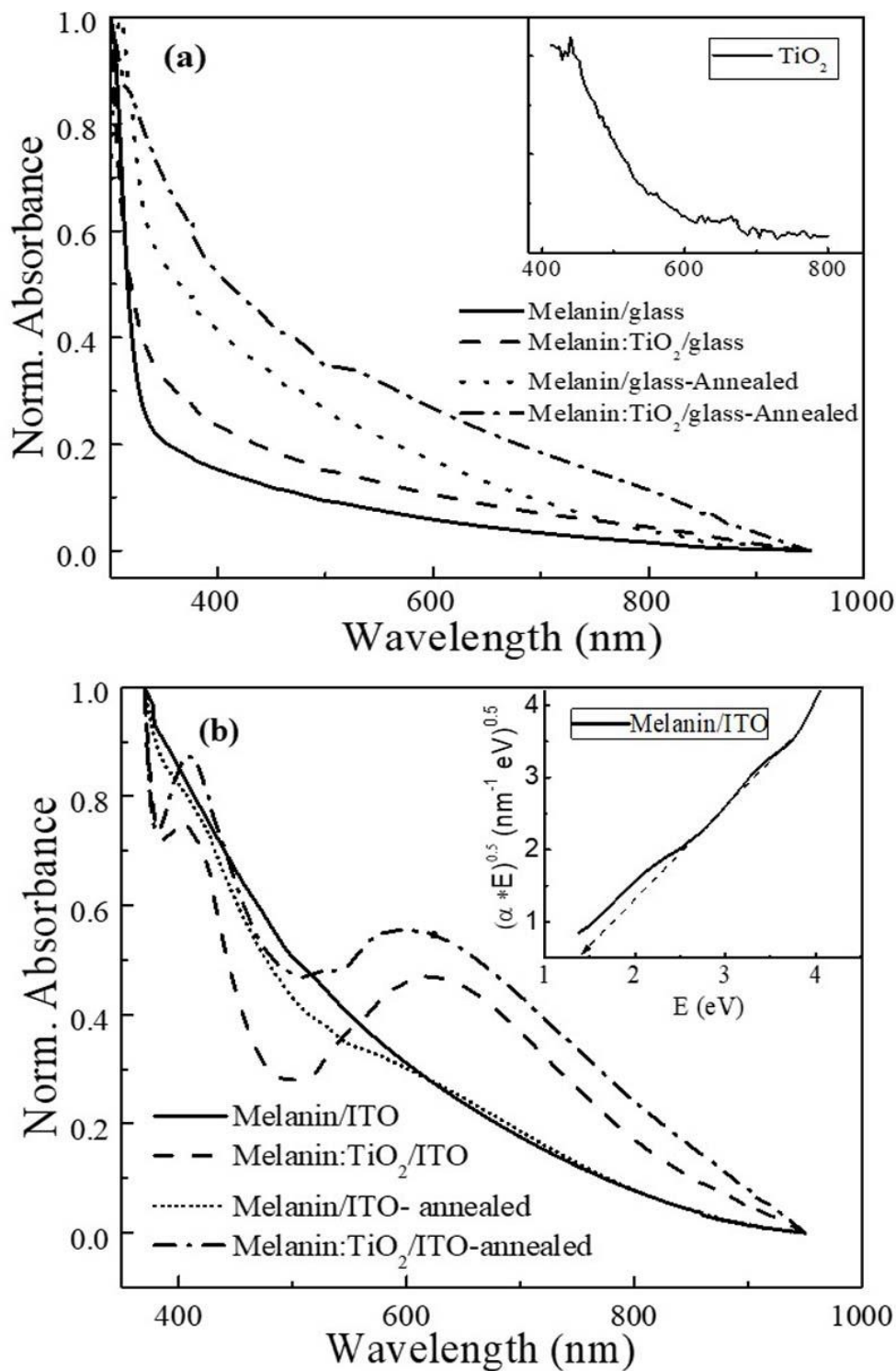
Fig. 5. Normalized absorption spectra of melanin and its blend (melanin: TiO_2) films on glass and on ITO substrates are shown in Fig. (a) and (b), respectively. The absorption spectra of TiO_2 nanoparticles deposited on ITO substrate by ESD deposition is reported in the inset of (a) and energy band edges of melanin film on ITO is described in the inset of (b), respectively.

255 more disordered natural melanin. Equation of the form $(\alpha h\nu)^{1/2} \propto (h\nu - E_g)$ according to the Tauc

256 model for indirect band gap semiconductor was used, where α is the absorption coefficient

257 (obtained from the absorption curves in Fig. 5), $h\nu$ is the incident photon energy on the sample,

258 and E_g gives the optical gap value by plotting the term $(\alpha h\nu)^{1/2}$ as a function of energy. The result

259 of extrapolated onset on the horizontal axis of the absorption curves for a set of all films in this

260 study was in the range of 1.25- 1.55 eV. The optical gap value 1.4 eV for melanin film deposited

261 on ITO substrates was obtained using the Tauc plot as shown in the inset of Fig. 5(b). The

262 estimated energy band gap values for melanin are slightly dependent on the choice of substrates,

263 annealing and on the interaction of TiO_2 nanoparticles as photocatalytic that induced stacking

264 ordering in the polymeric chains. These values are comparable to the melanin E_g values observed

265 in the range from 1.0 to 1.4 eV [4,6,24,30,32,33,34]. We must be aware of the effect of Mie

266 scattering that may be present at the longer wavelengths in the tail part of the spectra [3,4,6,9]

267 affecting the energy band edge.

3.3. Photoluminescence spectroscopy

269 To examine further the optical properties of melanin and blend films of melanin: TiO_2 a PL study

270 was carried out at room temperature in order to understand the interaction between the two

271 components. As a comparison, Fig. 6(a and b) show the PL spectra of melanin and blend thin

272 films excited with the excitation wavelength of 325 nm. It is found that different behavior of the

273 PL spectra in the range of 300– 950 nm before annealing supports the significant substrate

274 effects obtained previously from morphological and absorption analysis. The emission spectrum

275 for 325 nm (3.8 eV) excitation reached the peaks maximum at around 550 nm obtained from

276 melanin on glass substrates and then decreased monotonically with increasing emission

277 wavelength [32,35], while the emission spectrum for melanin: TiO_2 blend on glass substrates

278 (Fig. 6a) was reduced due to incorporation of the TiO_2 nanoparticles in the melanin matrix.

279   Similar emission spectra related to the DHICA anions were obtained with maximum peak

280 intensity at wavelength of 425 nm [19] compared to 550 nm in this case. Furthermore, it has

281 been shown in the literature that melanin PL quantum yield is small, proved by the probe beam

282 attenuation method and origin of some unexpected observations [7,26,36]. We supposed that the

283 reason of unforeseen wide PL (FWHM ~ 1eV) behavior of pure melanin and blend films, on

284 insulating substrates could be that the exciton emission originating from a hole-electron
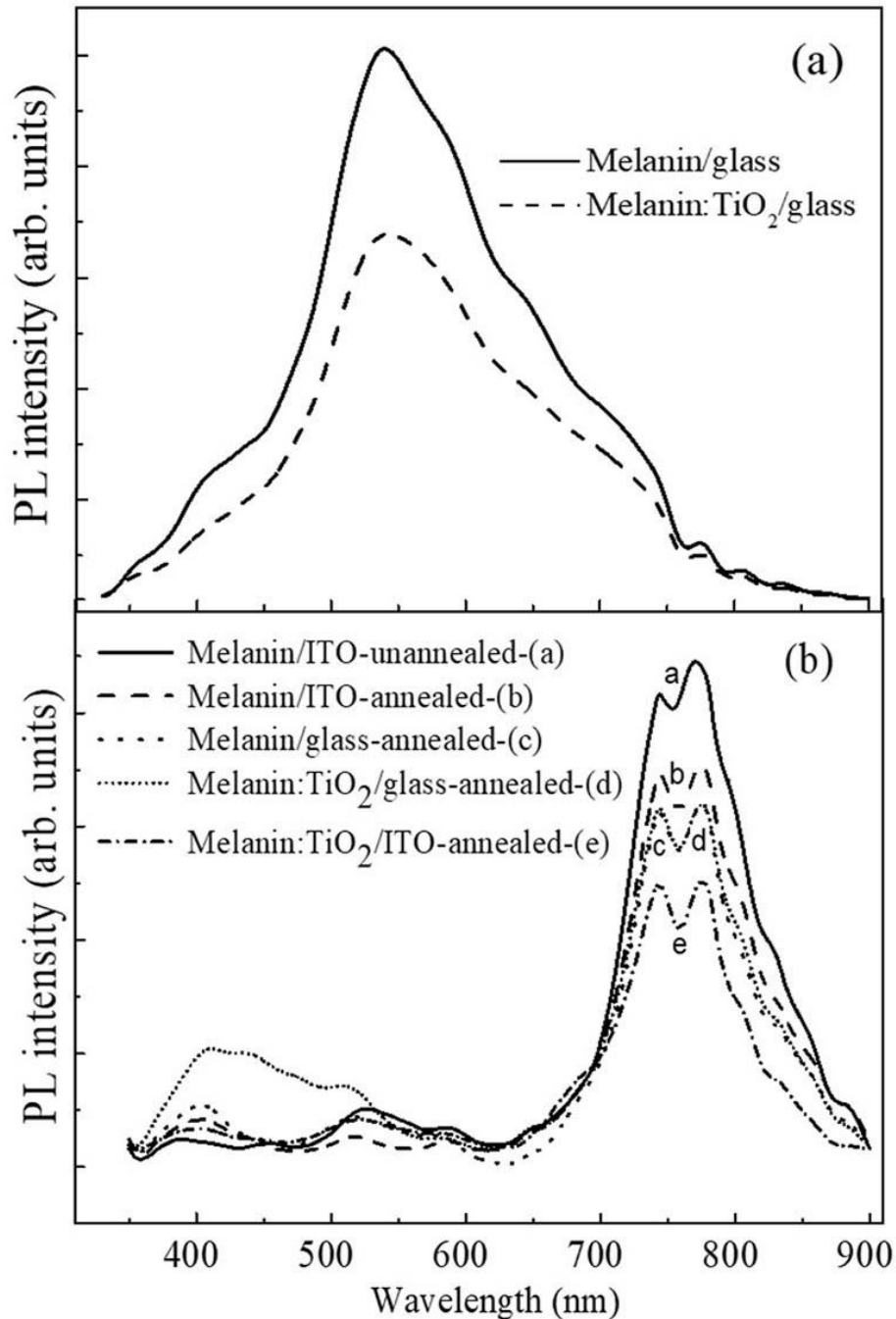
Fig. 6. (a) PL spectra of melanin and blend samples deposited on glass substrates before annealing. (b) PL spectra of melanin and hybrid melanin: TiO$_2$ samples deposited on insulating and conducting substrates before and after annealing at 120° C for 5 minutes. All PL spectra were recorded with He-Cd laser having excitation wavelength 325 nm (3.8 eV).

290   recombination, was most probably due to trapped states on the surface [15], resulting from the

291   combination of disorder of melanin monomers, defects (oxygen vacancies/structural defects due

292   to agglomeration) and impurities including two kinds of water bonded in structure of melanin.

293   Such impurities and defects could be eliminated by thermal, physical or chemical processes. In

294   the case of thin films of organic species such as melanin and its blend with TiO_2 anatase phase

295   over the ITO conductive (Fig. 6b) layer, electron and hole scavengers and the charge

296   recombination mechanism in the visible and up to near infrared region are dominant [26,37,38].

297   The PL spectra after annealing (Fig. 6b) for a set of samples were shifted to an energy gap values

298   near IR region (700- 900 nm) compared to that on glass substrates before annealing in the

299   wavelength range 350-550 nm. Such observations are suggesting that the recombination of a hole

300   with an electron due to surface trapped states/ disordering was reduced after annealing. The

301   intense peaks in overall spectra for melanin and titanium dioxide were observed at the high

302   wavelength near IR band gap region (Fig. 6b) for melanin, suggesting larger π-stacking

303   oligomerization related to red-shifts in the absorption spectra and then emission. The intense

304   excitation peaks in annealed PL emission spectra of the thin films started at offset of 1.3-1.45 eV

305   and reach their maximum at 1.55 eV. These observations are in agreement with the estimated

306   band gap values obtained from absorption analysis. The PL peaks (probably affected by

307   spectrometer background) in the range of 1.5- 1.65 eV may correspond to different

308   chromophores [3,7] of melanin DHI and DHICA, the latter one at lower energy compared to

309   DHI that has dissimilar reaction times and extinction coefficients at different wavelengths [39].

310   In the Fig. 6(b), these observations further elucidate the trend of PL peaks intensity that

311   quenched significantly in a systematic way from the pristine melanin/ITO film (curve-a) by

312   annealing the same sample (curve-b) and then by adding TiO_2 nanoparticles as an electron

313   acceptor with respect to the donor melanin material (curve-e). It reveals the strong interface

314   formation between melanin and TiO_2 nanoparticles as a nanohybrid structures fostering robust

315   devices applications. On the contrary, on insulating surface almost the same PL peaks intensity

316   for thin films of melanin/glass (curve-c) and the blend/glass (curve-d) are observed, suggesting

317   the weak interface formation between melanin and TiO_2 nanoparticles, that results in the TiO_2

318   nanoparticles PL response at around the wavelength values (450-550 nm).

319   To put into relation the absorption and PL spectra, we observed an increase in the absorbance

320   with dominants absorption feature for melanin: TiO_2 samples and unusual emission spectra from

321 PL spectroscopy. The comparison of annealed melanin: TiO_2/ITO absorbance (in Fig. 5(b),

322 dash-dot curve) and PL spectrum shown in Fig. 6 (curve-e) revealed our observations further.

323 Here, we must point out that efforts are required to quench completely the PL spectra for the

324 melanin-TiO_2 hybrid nanostructures peculiarly presented here in the near IR band gap region.

325 For such a complex nanohybrid system, this could be done in the future by balancing the charge

326 carrier mobilities while changing the ratio of melanin: TiO_2 (1:1) nanoparticles that will

327 eventually reduce charge recombination processes.

3.4. Raman and Fourier transform infrared spectroscopy

329 Raman spectra were collected from melanin and its blend with TiO_2 (Melanin: TiO_2) films which

330 were deposited on glass and ITO substrates through ESD technique. All ESD films investigated

331 through visual inspection with microscope and by Raman spectroscopic analysis were quite

332 homogenous, which permitted their study by a spatial resolution on the surface of the samples

333 around 1 μm [6]. The Raman spectra of melanin are similar to the amorphous carbon graphitic

334 structure having two dominant peaks at about 1600 cm^{-1} and 1300 cm^{-1}, which are related to the

335 vibrational modes. These vibrational modes involving different atoms (carbon, oxygen, nitrogen

336 and hydrogen) are organized according to different functional groups, bonded to indolic structure

337 that gives the formation of basic monomeric units of melanin such as DHI, DHICA, SQ and IQ.

338 The Raman spectra of thin films taken at room temperature consists of Raman active vibrational

339 modes involving these different functional groups like, hydroxyl groups OH, carbonyl groups

340 C=O, carboxylic acid COOH and NH groups, as reported in Fig. 7. In blended samples a slight

341 shift was observed in main G (~ 1600 cm^{-1}) and D band (~ 1300 cm^{-1}) of carbon structures due to

342 incorporation of TiO_2 nanoparticles of anatase phase. Moreover, the G and D band on ITO

343 substrates were more intense than on glass. The Raman spectrum was fitted using the Gaussian

344 function indicating the melanin (900-1800 cm^{-1}) and anatase TiO_2 (400-900 cm^{-1}) vibrational

345 modes. The enclosed fitted area of blended Raman spectrum is reported in the left inset of Fig.

346 7(a) that indicates the presence of TiO_2 nanoparticles modes in the range of 400-900 cm^{-1}. The

347 spectrum exhibit Raman fingerprints for anatase phase with important modes B_{1g} (419 cm^{-1}), A_{1g}

348 (517 cm^{-1}) and E_g (639 cm^{-1}) in agreement with previous results [40].

349 In the recent literature, nine and eleven components fitted Raman spectrum has been already

350 observed which were correlated with different vibrational modes of melanin [6,41]. In Fig. 7(a),

351
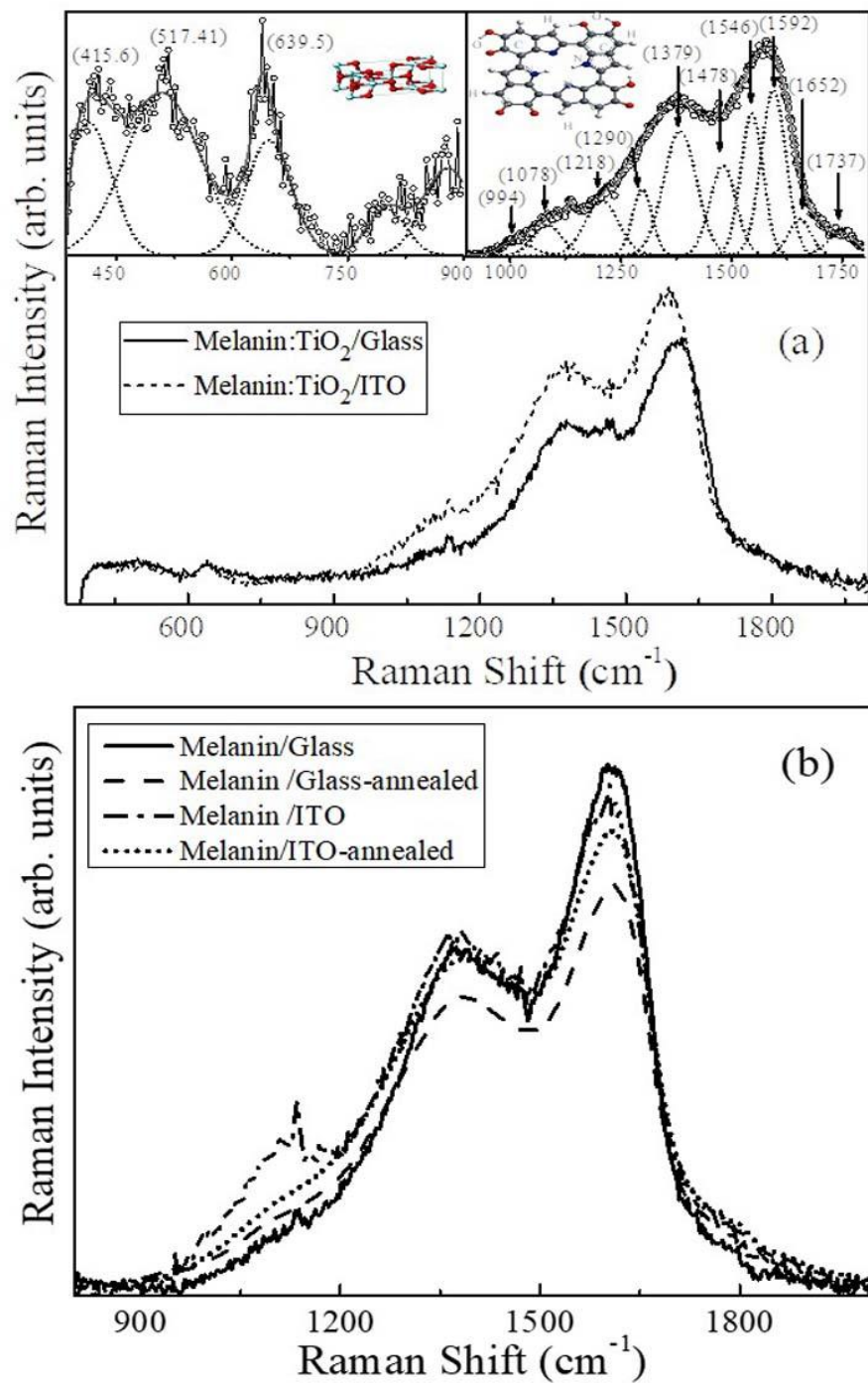
Fig. 7. (a) The normalized Raman spectra of blend (melanin: TiO_2) deposited on ITO and glass substrates, the inset showed the fitting plot of the experimental Raman spectrum along with chemical structure for both melanin (right) and TiO_2 (left), respectively. (b) Raman Spectra for melanin on ITO and glass substrates, before and after annealing of 120 ℃.

356

Table 1. Raman Peaks related with modes in melanin blended TiO_2 nanoparticles complex system.

Raman Peaks (cm-1)	Assignments
	Melanin Peaks in blend (melanin: TiO_2)
994 ± 2	O-H out of plane deformation
1078 ± 2	C-H deformation modes in or Out of plane
1218 ± 2	N-H in plane deformation and stretching C-C ring breathing
1290 ± 2	C-O stretching and OH deformation in COOH
1379 ± 2	Stretching (C-N)/indole ring vibration
1478 ± 2	C=C and C=N in plane vibration in pyrrole
1546 ± 2	Pyrrole ring stretching vibration/ C=C aromatic
1592 ± 2	Indole ring vibration / stretching antisymmetric (COO-)
652 ± 2	C=C aromatic ring vibration
1737 ± 2	Stretching C=O in DHICA, Quinone or Ketone
	TiO_2 Peaks in Blend
639 ± 2	E_g mode for anatase TiO_2
517 ± 2	A_{1g} mode for TiO_2
415 ± 2	B_{1g} mode for TiO_2

the Raman spectra of blended films confirmed that titania nanoparticles are not perturbing the spectral response of melanin functional group. The best-fitting curve of melanin experimental Raman spectrum composed of ten components is shown in the right inset (zoomed from solid curve) of Fig. 7(a). The peaks around 800 to 1000 cm^{-1} in the melanin structure are due to the deformation of modes of vibration in the pyrrole and indole structure. The broad peaks about 1400 cm^{-1} overlap different vibrational modes namely C=C, C=N ring stretching in pyrrole structure. The lower intensity bands around 900 – 1200 cm^{-1} are due to the vibration modes of CH, OH and NH with in plane or out of plane deformation. The broad band feature at 1550 and 1622 cm^{-1} is the contribution to the Raman bands of pyrrole and indole ring stretching vibrations. The peaks centered at about 1700 and 1775 cm^{-1} related to the C=O stretching vibrational modes in carboxylic acid or in quinone or ketone group. However, at 1775 cm^{-1} and above weak peaks are observed corresponding to the stretching of carbonyl functional group vibrations in carboxylic acid [42]. The pyrrole di- and tri-carboxylic groups are also investigated during the subsequent oxidization of DHI and DHICA, which described the structure of melanin [43].

389 These Gaussian peaks value corresponding to the various vibrational modes for melanin and
390 TiO$_2$ anatase peaks in the melanin: TiO$_2$ sample obtained from the fitting of the experimental
391 Raman spectrum are listed in Table 1.

392 On the other hand, Raman spectra of the melanin on glass and ITO substrates before and after
393 annealing are given in Fig. 7(b). It is important to note that the Raman spectrum of the melanin
394 on glass reflect the structure like graphitic amorphous carbon, with a band D at 1300 cm^{-1} and a
395 strong band G at 1600 cm^{-1} [6,41]. A small shift was observed in the G band position of melanin
396 spectra deposited on ITO compared to glass substrates, and after annealing compared to as
397 prepared melanin film on ITO. This regular small shift in the position of G strong band after
398 annealing of melanin Raman spectra is similar to aromatic character changing from amorphous
399 carbon graphitic structure to nanocrystalline diamond and/or nanocrystalline carbon graphitic
400 structure. Furthermore, the shift in the G position is related to the optical Tauc gap [44],
401 supporting our results obtained from absorption and PL analysis.

402 Fig. 8 depicts further the identification and investigation of functional group vibrations of
403 melanin and melanin: TiO$_2$ hybrid nanostructures with a more comprehensive spatial range
404 by using NICOLET 6700 Fourier Transform infrared spectroscopy (FTIR). The IR spectra
405 indicated clearly that the large absorption due to functional group of melanin and hybrid
406 melanin-TiO$_2$ nanostructures were characterized with different bonds in their respective regions
407 as depicted on top of Fig. 8. The peak values assigned to different modes of vibrations at 1150-
408 1371 due to C-C, C-O, and at 1460 cm^{-1} due to C-N vibrations are similar to the reported values
409 in references [45]. A wide band centered at ~3000 cm^{-1} in both spectra was observed, which is
410 corresponding to O-H stretching due to the presence of water in the melanin structure. IR
411 absorption peaks in the range of 1460- 1730 cm^{-1} are assigned to the bonding vibrations of C=C,
412 C=O and to the stretching of COOH double bonds. Moreover, in the blend thin film (melanin:
413 TiO$_2$) the broad peaks observed at 3450-2400, 1609 and 720 cm^{-1} were ascribed to the presence
414 of OH, C=O and Ti–O in the catalyst, and is suggesting the oxidative polymerization in the
415 formation of hybrid nanostructure [46].

416
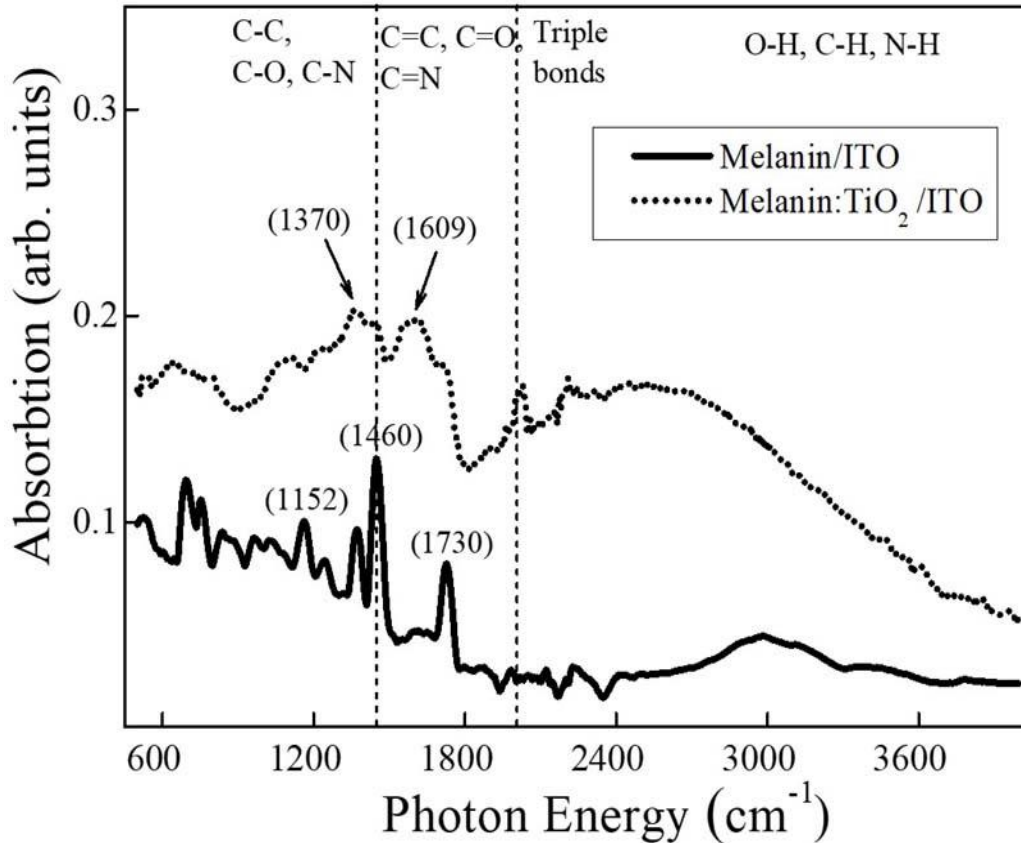
Fig. 8. IR absorption spectra of melanin thin films (lower-solid curve) and melanin: TiO$_2$ thin films (upper-dot curve) deposited by controlled ESD methods.

3.5. Electrical characterization

The charge transport characteristics of ESD synthetic melanin blended with TiO$_2$ nanoparticles films were measured under nitrogen- gas condition to avoid any surrounding effects. In Fig. 9 the Current–Voltage (J –V) curves were obtained by using a Keithley 4200 semiconductor analyzer in dark and under illumination of an AM1.5 (100 mW/cm^2) calibrated with IL1400BL radiometer. Gold stripes were evaporated with a channel length of 50μm onto 7059 Corning glass substrates after film deposition to get planar geometry for J – V measurements in both forward and backward voltage sweep directions. In principle, more detailed analysis and improved performance could be obtained in the future by sandwiching the blended layer between two electrodes for an ideal devices modeling. At room temperature, the hysteretic behavior of melanin: TiO$_2$ films as shown in Fig. 9, contracted noticeably compared with hysteretic behavior that was reported in the previous work of ESD melanin films [6], due to the presence of shallow

431 trap states and to the existence of two types of water weakly and strongly bounded in melanin

432 pores structures [9,12].

433 Previously, it was described that the electrical transport across the melanin active layers could

434 strongly be affected by hydration state [3,5,9,12] Such effects in the J-V curve for hybrid

435 nanostructures layer were compensated by the presence of TiO_2 as an electron acceptor in the

436 melanin matrix by filling the pores structures, while in case of ESD melanin films these trapped

437 charges were released due to phonon-assisted hopping with increase in temperature. Moreover,

438 the photocatalytic and water splitting characteristics of TiO_2 played crucial role to alter the

439 hydration state for melanin charge transport mechanism in a reorganized structure. To assess the

440 photo response of such active layer for organic/inorganic solar cells, the J-V curves for melanin:

441 TiO_2 films under illumination were obtained. We found a strong photo response in the

442 photoactive layer of melanin: TiO_2 thin film. The resistance of ESD melanin: TiO_2 film is very

443 low at room temperature compared with ESD melanin films [9]. It is worth to note that TiO_2

444 nanoparticles as an electron acceptor semiconducting materials probably enhanced the charge

445 transport towards electrodes by the reduced charge recombination effect in the active layer when

446

447
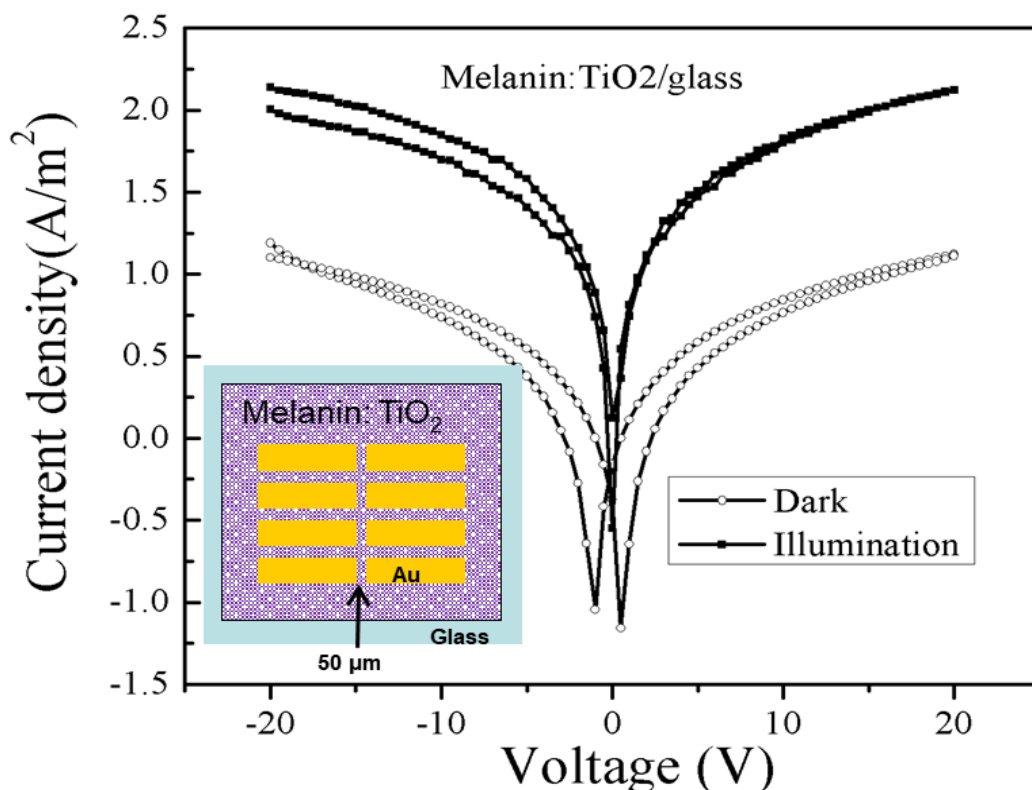
Fig. 9. J-V curve of a planar blend (melanin: TiO_2) structure both in forward and backward voltage sweep directions, measured by two Au electrodes separated by 50 μm. In the inset a planar geometry for J-V measurements on glass is shown.

added with melanin. These results are in agreement with optical, morphological and structural analysis, and revealed that hybrid melanin: TiO_2 nanostructures are active semiconducting agents that can be employed as potential biocompatible nanomaterials in organic/inorganic bio/ (opto)electronic devices technology.

4 Conclusions

In this work, we described the formation of hybrid nanostructures of melanin with TiO_2 nanoparticles by ESD technique. Morphological analysis of the ESD thin films revealed quite homogeneous and uniform flat surfaces covering the complete substrate area. After subsequent thermal annealing, the oligomeric aggregates characteristic of melanin, as well as the hybrid nanostructures interfaces area are increased due to the mild distribution of titania particles in the melanin matrix and the strong adhesion between them that strongly influenced the physico-chemical properties. The broadband absorption of the melanin: TiO_2 hybrid films also increased as a result of the interaction of TiO_2, nanoparticles especially on the conducting substrates. In fact, after heat treatments the absorption features in the optical absorption and PL characteristics of melanin: TiO_2 layers on ITO substrates were enhanced. These facts preannounced the reorganized growth mechanism of self-assembled supramolecular structures with increasing degree of oligomerization and π-stacking of oligomers. In our opinion this result opens the way to a possible tuning of the band gap values and increase in the External Quantum Efficiency (EQE) in the infrared range of wavelengths. However, further quenching of the PL broad emission peaks is still an open issue for experimental researchers to balance the charge carrier mobility of optoelectronic devices with higher efficiency. These experimental results including: efficient charge transport mechanism, rationalized feature of absorption and quenching of PL emission, robust formation of melanin: TiO_2 hybrid nanostructures (elucidated by Raman and IR spectroscopies), represent a significant step toward future implementations of optoelectronic and bio-electronic/sensor devices using this important bio-polymer. .

Acknowledgments

Author Information

*E-mail:mushtaqali.zada@gmail.com (M Ali)

REFERENCES

[1]   M. D'Ischia, A. Napolitano, A. Pezzella, P. Meredith, T. Sarna, Chemical and structural diversity in eumelanins: Unexplored bio-optoelectronic materials, Angew. Chemie - Int. Ed. 48 (2009) 3914–3921. https://doi:10.1002/anie.200803786.

[2]   P. Meredith, T. Sarna, The physical and chemical properties of eumelanin, Pigment Cell Res. 19 (2006) 572–594. https://doi.org/10.1111/j.1600-0749.2006.00345.x.

[3]   M. Ambrico, P.F. Ambrico, T. Ligonzo, A. Cardone, S.R. Cicco, M. D'Ischia, G.M. Farinola, From commercial tyrosine polymers to a tailored polydopamine platform: Concepts, issues and challenges en route to melanin-based bioelectronics, J. Mater. Chem. C. 3 (2015) 6413–6423. https://doi:10.1039/c5tc00570a.

[4]   C. Bonavolontà, C. De Lisio, M. D'Ischia, P. Maddalena, P. Manini, A. Pezzella, M. Valentino, Anomalous evolution of broadband optical absorption reveals dynamic solid state reorganization during eumelanin build-up in thin films, Sci. Rep. 7 (2017) 1–8. https://doi:10.1038/s41598-017-00597-8.

[5]   J. Wünsche, F. Cicoira, C.F.O. Graeff, C. Santato, Eumelanin thin films: Solution-processing, growth, and charge transport properties, J. Mater. Chem. B. 1 (2013) 3836–3842. https://doi:10.1039/c3tb20630k.

504 [6] M. Abbas, M. Ali, S.K. Shah, F. D'Amico, P. Postorino, S. Mangialardo, M.C. Guidi, A.
505 Cricenti, R. Gunnella, Control of structural, electronic, and optical properties of
506 eumelanin films by electrospray deposition, J. Phys. Chem. B. 115 (2011) 11199–11207.
507 https://doi:10.1021/jp2033577.

508 [7] P. Meredith, B.J. Powell, J. Riesz, S.P. Nighswander-Rempel, M.R. Pederson, E.G.
509 Moore, Towards structure-property-function relationships for eumelanin, Soft Matter. 2
510 (2006) 37–44. https://doi:10.1039/b511922g.

511 [8] J.P. Bothma, J. De Boor, U. Divakar, P.E. Schwenn, P. Meredith, Device-quality
512 electrically conducting melanin thin films, Adv. Mater. 20 (2008) 3539–3542.
513 https://doi:10.1002/adma.200703141.

514 [9] M. Abbas, F. D'Amico, L. Morresi, N. Pinto, M. Ficcadenti, R. Natali, L. Ottaviano, M.
515 Passacantando, M. Cuccioloni, M. Angeletti, R. Gunnella, Structural, electrical,
516 electronic and optical properties of melanin films, Eur. Phys. J. E. 28 (2009) 285–291.
517 https://doi:10.1140/epje/i2008-10437-9.

518 [10] M. Ambrico, A. Cardone, T. Ligonzo, V. Augelli, P.F. Ambrico, S. Cicco, G.M. Farinola,
519 M. Filannino, G. Perna, V. Capozzi, Hysteresis-type current-voltage characteristics in
520 Au/eumelanin/ITO/glass structure: Towards melanin based memory devices, Org.
521 Electron. 11 (2010) 1809–1814. https://doi:10.1016/j.orgel.2010.08.001.

522 [11] S.R. Cicco, M. Ambrico, P.F. Ambrico, M.M. Talamo, A. Cardone, T. Ligonzo, R. Di
523 Mundo, C. Giannini, T. Sibillano, G.M. Farinola, P. Manini, A water-soluble eumelanin
524 polymer with typical polyelectrolyte behaviour by triethyleneglycol N-functionalization,
525 J. Mater. Chem. C. 3 (2015) 2810–2816. https://doi:10.1039/c4tc01997k.

526 [12] M. Ambrico, P.F. Ambrico, T. Ligonzo, A. Cardone, S.R. Cicco, A. Lavizzera, V.
527 Augelli, G.M. Farinola, Memory-like behavior as a feature of electrical signal
528 transmission in melanin-like bio-polymers, Appl. Phys. Lett. 100 (2012) 253702.
529 https://doi:10.1063/1.4729754.

530 [13] M. Ambrico, P.F. Ambrico, A. Cardone, T. Ligonzo, S.R. Cicco, R. Di Mundo, V.
531 Augelli, G.M. Farinola, Melanin layer on silicon: An attractive structure for a possible
532 exploitation in bio-polymer based metal-insulator-silicon devices, Adv. Mater. 23 (2011)
533 3332–3336. https://doi:10.1002/adma.201101358.

[14]   A. Fakharuddin, F. Di Giacomo, A.L. Palma, F. Matteocci, I. Ahmed, S. Razza, A. D'Epifanio, S. Licoccia, J. Ismail, A. Di Carlo, T.M. Brown, Vertical TiO$_2$ Nanorods as a Medium for Stable and High-Efficiency Perovskite Solar Modules, ACS Nano. 9 (2015) 8420–8429. https://doi:10.1021/acsnano.5b03265.

[15]   J. Boucle, S. Chyla, M.S.P. Shaffer, J.R. Durrant, D.D.C. Bradley, J. Nelson, Hybrid solar cells from a blend of poly (3-hexylthiophene) and ligand-capped TiO2 nanorods, Adv. Funct. Mater. 18 (2008) 622–633. https://doi.org/10.1002/adfm.200700280.

[16]   U.M. Garusinghe, V.S. Raghuwanshi, W. Batchelor, G. Garnier, Water Resistant Cellulose-Titanium Dioxide Composites for Photocatalysis, Sci. Rep. 8 (2018) 2306. https://doi:10.1038/s41598-018-20569-w.

[17]   H. J. Nam, B. Kim, M. J. Ko, M. Jin, J. M. Kim, and D.-Y. Jung, A New Mussel-Inspired Polydopamine Sensitizer for Dye-Sensitized Solar Cells: Controlled Synthesis and Charge Transfer, Chem. Eur. J. 2012, 18, 14000 – 14007. https://doi: 10.1002/chem. 201202283

[18]   G. Vitiello, A. Pezzella, A. Zanfardino, B. Silvestri, P. Giudicianni, A. Costantini, M. Varcamonti, F. Branda, G. Luciani, Antimicrobial activity of eumelanin-based hybrids: The role of TiO2 in modulating the structure and biological performance, Mater. Sci. Eng. C. 75 (2017) 454–462. https://doi.org/10.1016/j.msec.2016.12.135.

[19]   G. Vitiello, A. Pezzella, V. Calcagno, B. Silvestri, L. Raiola, G. D'Errico, A. Costantini, F. Branda, G. Luciani, 5,6-Dihydroxyindole-2-carboxylic Acid–TiO 2 Charge Transfer Complexes in the Radical Polymerization of Melanogenic Precursor(s), J. Phys. Chem. C. 120 (2016) 6262–6268. https://doi:10.1021/acs.jpcc.6b00226.

[20]   M. Ali, M. Abbas, S.K. Shah, E. Bontempi, P. Colombi, A. Di Cicco, R. Gunnella, Variability of physical characteristics of electro-sprayed poly (3-hexylthiophene) thin films, Journal of Applied Physics. 054515 (2011) 1–9. https://doi:10.1063/1.3633519.

[21]   M. Ali, M. Abbas, S.K. Shah, R. Tuerhong, A. Generosi, B. Paci, L. Hirsch, R. Gunnella, Realization of solution processed multi-layer bulk heterojunction organic solar cells by electro-spray deposition, Org. Electronics. 13 (2012) 2130–2137. https://doi:10.1016/j.orgel.2012.06.016.

[22]   D. Nečas, P. Klapetek, Gwyddion: an open-source software for SPM data analysis, Open Physics. 10 (2012) 181–188. https://doi:10.2478/s11534-011-0096-2.

565 [23]   G.S. Lorite, V.R. Coluci, M.I.N. Da Silva, S.N. Dezidrio, C.F.O. Graeff, D.S. Galvão,
566   M.A. Cotta, Synthetic melanin films: Assembling mechanisms, scaling behavior, and
567   structural properties, J. Appl. Phys. 99 (2006) 113511. https://doi:10.1063/1.2200401.

568 [24]   T. Ligonzo, M. Ambrico, V. Augelli, G. Perna, L. Schiavulli, M.A. Tamma, P.F. Biagi,
569   A. Minafra, V. Capozzi, Electrical and optical properties of natural and synthetic melanin
570   biopolymer, J. Non. Cryst. Solids. 355 (2009) 1221–1226.
571   https://doi.org/10.1016/j.jnoncrysol.2009.05.014.

572 [25]   R. Mosurkal, Jin-An He, K. Yang, L. A. Samuelson, J. Kumar, Organic photosensitizers
573   with catechol groups for dye-sensitized photovoltaics, J. of Photochemistry and
574   Photobiology A: Chemistry 168 (2004) 191–196. https://doi.org/10.1016/j.
575   jphotochem.2004.05.004

576

577 [26]   S.P. Nighswander-Rempel, J. Riesz, J. Gilmore, J.P. Bothma, P. Meredith, Quantitative
578   Fluorescence Excitation Spectra of Synthetic Eumelanin, J. Phys. Chem. B. 109 (2005)
579   20629–20635. https://doi:10.1021/jp053704+.

580 [27]   M. Ali, M. Abas, S.K. Shah, E. Bontempi, A. Di Cicco, R. Gunnella, Film forming
581   properties of electrosprayed organic heterojunctions, Eur. Phys. Appl. Phys. 62 (2013)
582   30202. https://doi:10.1051/epjap/2013130107.

583 [28]   D. Tuna, A. Udvarhelyi, A.L. Sobolewski, W. Domcke, T. Domratcheva, Onset of the
584   electronic absorption spectra of isolated and π-stacked oligomers of 5, 6-
585   dihydroxyindole: An ab initio study of the building blocks of eumelanin, J. Phys. Chem.
586   B. 120 (2016) 3493–3502. https://doi.org/10.1021/acs.jpcb.6b01793

587 [29]   K.B. Stark, J.M. Gallas, G.W. Zajac, J.T. Golab, S. Gidanian, T. McIntire, P.J. Farmer,
588   Effect of stacking and redox state on optical absorption spectra of melanins -- comparison
589   of theoretical and experimental results., J. Phys. Chem. B. 109 (2005) 1970–1977.
590   https://doi:10.1021/jp046710z.

591 [30]   L. Sangaletti, P. Borghetti, P. Ghosh, S. Pagliara, P. Vilmercati, C. Castellarin-Cudia, L.
592   Floreano, A. Cossaro, A. Verdini, R. Gebauer, A. Goldoni, Polymerization effects and
593   localized electronic states in condensed-phase eumelanin, Phys. Rev. B. 80 (2009)
594   174203. https://doi:10.1103/PhysRevB.80.174203.

595 [31] I.G. Kim, H.J. Nam, H.J. Ahn, D.Y. Jung, Electrochemical growth of synthetic melanin
596   thin films by constant potential methods, Electrochim. Acta. 56 (2011) 2954–2959.
597   https://doi:10.1016/j.electacta.2010.12.095.

598 [32] T. Eom, K. Woo, B.S. Shim, Melanin: A naturally existing multifunctional material,
599   Appl. Chem. Eng. 27 (2016) 115–122. https://doi:10.14478/ace.2016.1029.

600 [33] V. Capozzi, G. Perna, A. Gallone, P.F. Biagi, P. Carmone, A. Fratello, G. Guida, P.
601   Zanna, R. Cicero, Raman and optical spectroscopy of eumelanin films, J. Mol. Struct.
602   744–747 (2005) 717–721. https://doi:10.1016/j.molstruc.2004.11.074.

603 [34] L. Sangaletti, S. Pagliara, P. Vilmercati, C. Castellarin-Cudia, P. Borghetti, P. Galinetto,
604   R. Gebauer, A. Goldoni, Electronic excitations in synthetic eumelanin aggregates probed
605   by soft X-ray spectroscopies, J. Phys. Chem. B. 111 (2007) 5372–5376.
606   https://doi:10.1021/jp067415c.

607 [35] G. Perna, G. Palazzo, A. Mallardi, V. Capozzi, Fluorescence properties of natural
608   eumelanin biopolymer, J. Lumin. 131 (2011) 1584–1588.
609   https://doi:10.1016/j.jlumin.2011.03.055.

610 [36] J.B. Nofsinger, T. Ye, J.D. Simon, Ultrafast Nonradiative Relaxation Dynamics of
611   Eumelanin, J. Phys. Chem. B. 105 (2001) 2864–2866. https://doi:10.1021/JP004045Y.

612 [37] J.V. Paulin, A.G. Veiga, Y. Garcia-Basabe, M.L.M. Rocco, C.F.O. Graeff, Structural and
613   optical properties of soluble melanin analogues with enhanced photoluminescence
614   quantum efficiency, Polym. Int. 67 (2018) 550–556. https://doi:10.1002/pi.5543.

615 [38] S. Zhu, Y. Song, X. Zhao, J. Shao, J. Zhang, B. Yang, The photoluminescence
616   mechanism in carbon dots (graphene quantum dots, carbon nanodots, and polymer dots):
617   current state and future perspective, Nano Res. 8 (2015) 355–381. https://doi
618   10.1007/s12274-014-0644-3.

619 [39] R. Micillo, L. Panzella, M. Iacomino, G. Prampolini, I. Cacelli, A. Ferretti, O. Crescenzi,
620   K. Koike, A. Napolitano, M. D'Ischia, Eumelanin broadband absorption develops from
621   aggregation-modulated chromophore interactions under structural and redox control, Sci.
622   Rep. 7 (2017) 41532. https://doi:10.1038/srep41532.

623 [40] N. Farahani, P. Kelly, G. West, M. Ratova, C. Hill, V. Vishnyakov, An Investigation into
624   W or Nb or ZnFe2O4 Doped Titania Nanocomposites Deposited from Blended Powder

Targets for UV/Visible Photocatalysis, Coatings. 3 (2013) 153–165. https://doi:10.3390/coatings3030153.

[41] G. Perna, M. Lasalvia, C. Gallo, G. Quartucci, V. Capozzi, Vibrational Characterization of Synthetic Eumelanin by Means of Raman and Surface Enhanced Raman Scattering, Open Surf. Sci. J. 5 (2013) 1–8. https://doi:10.2174/1876531901305010001.

[42] F. Rossella, P. Galinetto, M.C. Mozzati, L. Malavasi, Y. Diaz Fernandez, G. Drera, L. Sangaletti, TiO2 thin films for spintronics application: a Raman study, J. Raman Spectrosc. An Int. J. Orig. Work All Asp. Raman Spectrosc. Incl. High. Order Process. Also Brillouin Rayleigh Scatt. 41 (2010) 558–565. https://doi.org/10.1002/jrs.2465.

[43] S.A. Centeno, J. Shamir, Surface enhanced Raman scattering (SERS) and FTIR characterization of the sepia melanin pigment used in works of art, J. Mol. Struct. 873 (2008) 149–159. https://doi.org/10.1016/j.molstruc.2007.03.026.

[44] A.C. Ferrari, J. Robertson, Interpretation of Raman spectra of disordered and amorphous carbon, Phys. Rev. B. 61 (2000) 14095. https://doi.org/10.1103/PhysRevB.61.14095.

[45] H. Okuda, A. Nakamura, K. Wakamatsu, S. Ito, T. Sota, Mid-infrared absorption spectrum of 5, 6-dihydroxyindole-2-carboxylic acid, Chem. Phys. Lett. 433 (2007) 355–359. https://doi.org/10.1016/j.cplett.2006.11.058.

[46] B. Erdem, R.A. Hunsicker, G.W. Simmons, E.D. Sudol, V.L. Dimonie, M.S. El-Aasser, XPS and FTIR Surface Characterization of TiO_2 Particles Used in Polymer Encapsulation, Langmuir. 17 (2001) 2664–2669. https://doi:10.1021/la0015213.

*Credit Author Statement

Mushtaq Ali: Conceptualization   Muhammad Saad: Data Curation Mamatimin Abbas: Editing Arshad S. Bhatti Reviewing and Editing Luca Ottaviano   Reviewing and Editiong Marianna Ambrico Sample preparation   Andrea Di Cicco Revision, , and Roberto Gunnella: Experimental growth method, Reviewing and editing

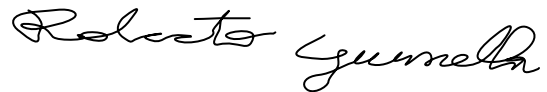***Declaration of Interest Statement**

Declaration of interests

X The authors declare that they have no known competing financial interests or personal relationships that could have appeared to influence the work reported in this paper.

X The authors declare the following financial interests/personal relationships which may be considered as potential competing interests:

Camerino 19/07/2020
Roberto Gunnella